The effect of reduced pressure on the characteristics of spreading flames

Luca Carmignani¹, Michael J. Gollner² and Carlos Fernandez-Pello³ *University of California, Berkeley, Berkeley, 94720, USA*

Maria Thomsen⁴ Universidad Adolfo Ibáñez, Santiago, Chile

Sonia Fereres ⁵ *Abengoa Innovación, Sevilla, 41014, Spain*

and

David Urban⁶ and Gary A. Ruff⁷ NASA Glenn Research Center, Cleveland, OH, 44135, USA

Flame spread over solid fuels is a canonical problem in fire science, due to its direct implications on material flammability and importance in fire development. In a microgravity environment, such as onboard a spacecraft, flames can behave very differently than on Earth. This is concerning for spaceflight life safety, especially in higher-oxygen environments. Due to the difficulties associated with microgravity testing, low-pressure environments have been proposed as an alternative to approximately replicate the burning behavior of solid fuels observed in reduced gravity conditions because of similar diffusion and heat transfer mechanisms. However, the roles played by gravity and pressure on flame length, standoff distance, and flame spread rate vary with the burning configuration. In concurrent flame spread, the buoyant flow enhances the spread rate by bringing the flame closer to the fuel surface and increasing the heating of the solid fuel. In opposed flame spread, the sample is preheated by the flame ahead of the flame leading edge, which is strongly affected by the surrounding flow field. In this work, we consider flames spreading over thin cotton samples in both downward (opposed) and upward (concurrent) configurations to investigate the effect of pressure (30-100 kPa) on flame characteristics, such as spread rate and standoff distance. A small forced flow is induced upward so that the flames are exposed to a mixed (forced and free) flow. By reducing pressure, flames become less bright, their standoff distance increases, and their spread rates decrease similar to what is observed in low-gravity environments. These results could in help understanding the differences between flames spreading at low pressure and low gravity environments for these similar, yet very different, spreading configurations. They could also provide more information about potential Earth-based flammability testing of materials for spacecraft applications.

¹ Postdoctoral researcher, Mechanical Engineering Dept., 60 Hesse Hall, Berkeley, CA, 94720.

² Assistant Professor and Deb Faculty Fellow, Mechanical Engineering, 6105A Etcheverry Hall, Berkeley, CA, 94720.

³ Professor of the Graduate School, Mechanical Engineering, Berkeley, CA, 94720.

⁴ Faculty of Engineering and Science, Diagonal Las Torres 2640, Peñalolén, Santiago, Chile.

⁵ Engineer, Aerospace & Defense Division, Energía Solar 1, 41014 Sevilla, Spain

⁶ Branch Chief, Low-Gravity Exploration Technology Branch, MS 77-5, 21000 Brookpark Road, Cleveland, OH 44135

⁷Spacecraft Fire Safety Demonstration Project Manager, Exploration Systems Office, MS 162-7, 21000 Brookpark Road, Cleveland, OH 44135.

I. Introduction

FLAME spread over solid fuels has been studied for decades because of its importance in fire safety. The nature of a fuel, the conditions under which it ignites and burns, and its interactions with the surroundings determine the rate of growth and heat released by the fire. In confined habitats, especially when escape routes are not available and ventilation is limited, such as onboard a spacecraft, a fire or even a small flame could have catastrophic consequences. This is increasingly relevant as we look towards long duration space flight and the potential of reduced pressure, increased oxygen concentrations atmospheres (Space Exploration Atmospheres, SEA)¹. Therefore, understanding the physics behind spreading flames is important for life and habitat safety aboard spacecraft.

On Earth gravity, flames naturally generate their own flow fields as buoyancy induces upward currents proportional to the density difference between hot post-combustion gaseous products and the ambient air. In microgravity this buoyant flow field is extremely weak and comparable to diffusive flows, and flames may not spread without externally generated flows, such as the low velocity flows generated in spacecraft by heating, ventilation, and cooling systems (HVAC). Spreading flames are generally divided into two main categories: concurrent flame spread, where the direction of propagation is the same as that of an oncoming flow field, including upward-spreading flames on Earth, and counter-current or opposed-flow flame spread, where the flame moves against an incoming flow. Concurrent-flow flame spread is known to be more hazardous than opposed-flow flame spread in a terrestrial environment. Concurrent spread is characterized by an acceleratory portion in which the flame grows over the flammable material due to the increased buoyancy induced flows caused by the larger surface burning. However, it has been shown that in a low-gravity environment opposed-flow flames can grow more easily than concurrent spreading flames because of a fresh supply of oxidizer², and sometimes burn under conditions where extinguishment would occur on Earth³⁻⁵.

The challenges associated with microgravity experiments (cost, duration, safety regulations, among others) make testing in space or other microgravity facilities difficult, so researchers have to look at alternative methods to test the flammability of materials to be used in spacecraft environments. A possible approach is to use reduced ambient pressure, and consequently reduced density, to reproduce the burning characteristics observed in microgravity conditions. As the pressure is reduced, flames tend to move away from the fuel surface, and the boundary layer along the solid fuel becomes thicker⁶. Furthermore, this behavior causes a reduced heating of the fuel surface by the flame, that results in lower spread rate and flame length. Thus, the effect of reducing the ambient pressure has similar consequences as reducing the buoyant flow velocity in low gravity. Previous experiments suggest that reduced pressures ranging between 20-40 kPa may be able to simulate concurrent flames in microgravity in terms of flame spread rate and flame length⁷⁻⁹, at least for thin combustible materials. Furthermore, models involving a constant Grashof number have been successful in correlating partial gravity results¹⁰. However, there are some limitations to the comparison between low gravity and low pressure. Numerical studies and scaling analyses highlighted the importance of radiation losses in reduced pressure environments¹¹⁻¹³. At the same time, diffusion processes become more important because of the lower molecular density. This, in combination with different heating mechanisms and pressure effects on chemical kinetics, can change the flame structure¹⁴⁻¹⁸.

The comparison between concurrent flame spread rates over fabric and acrylic fuels at reduced pressure on Earth and in microgravity has given promising results when a mixed flow field is considered (given by a buoyant component depending on pressure and gravity and a forced component)^{7,8,10}. However, similar models have not been effective in comparing the terrestrial and microgravity results for opposed flame spread over acrylic rods¹⁹, suggesting that the heat transfer from the flame to the solid fuel is affected differently in this flame spread configuration. The different behavior of opposed and concurrent flames could be due to the different role played by the problem geometry; in concurrent flame spread, the flame develops from the upstream sample edge, and covers a large portion of the fuel (generally increasing in time). On the other hand, opposed-spreading flames develops from the downstream edge of the sample, preheating only the fuel ahead of the flame leading edge. This makes the opposed flames much slower, and usually steady, but also more susceptible to the ambient conditions such as flow velocity.

The comparison between low gravity and low pressure flame spread needs to account for differences related to the heat transfer mechanisms (i.e. heating of fuel surface, and importance of radiation), flow field (importance of buoyancy), and chemical kinetics, and these factors can play different roles based on the flame spread configuration. In this work, we compare the effect of reduced pressure on opposed and concurrent flames spreading over thin cotton samples. Specifically, we present flame spread rate, standoff distance and flame length variations with pressure. A previously developed theoretical analysis is expanded to study the correlation between predicted and measured standoff distance; opposed and concurrent spreading flames show a similar trend when reasonable length scales are

used for the prediction. These results should help further the understanding the effect of pressure on the heating of the fuel surface.

II. Experimental setup

The normal gravity experiments were conducted in an apparatus previously developed to study the flammability of solid combustible materials under varied ambient conditions^{7,8}. The apparatus consists of a laboratory scale combustion tunnel that is inserted in a pressure chamber (Figure 1). The tunnel has a 125 mm square cross section and a 600 mm total length. The first 350 mm section of the duct serves as a flow straightener, the other 250 mm segment of the duct is used as the test section. The

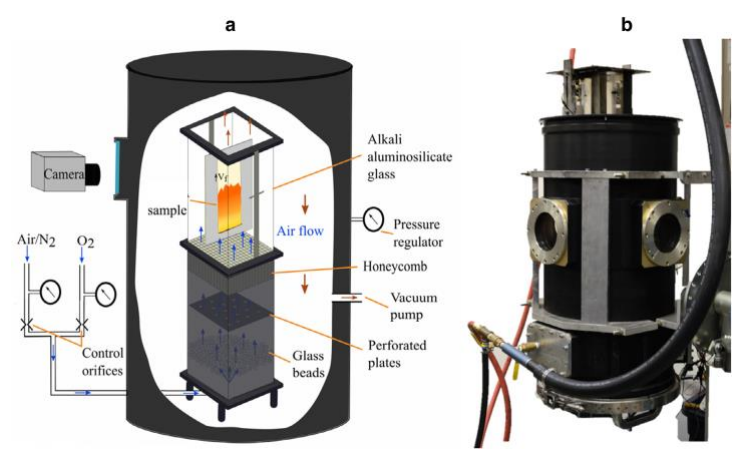


Figure 1. (a) Schematic of experimental apparatus and (b) picture of the exterior of the vacuum chamber.

chamber is provided with a flow system that provides constant supply and exhaust of gases to avoid vitiation problems. Compressed house air was supplied through critical nozzles (O'Keefe Controls) to the bottom of the duct while constantly evacuating to maintain constant pressure inside the chamber. The chamber pressure was controlled by a high-capacity vacuum generator (Vaccon JS-300) and a mechanical vacuum regulator. The chamber pressure was monitored constantly with an electronic pressure transducer (Omega Engineering, Inc. PX303-015A5V). The tests were conducted in air under pressures ranging between 30 and 100 ± 2 kPa. The forced flow was adjusted to provide 20 cm/s at the respective chamber pressure for all tests, this velocity was selected to match the flow of air induced by the HVAC system inside of a spacecraft. In addition to the forced flow, because the experiments were performed under Earth's gravity, the flame is also exposed to a self-induced buoyant flow. Thus, during the experiments the flame is exposed to a mixed (free and forced) flow condition.

The direction of the flow was upward, with the flames spreading downward (in opposed flow configuration) by igniting the sample at the top, and upward (in concurrent flow configuration) by igniting the sample at the bottom. The samples consisted of thin cotton fabric made out of pure cotton and had an overall area density of 21.8 mg/cm². The rectangular samples were held in between two identical stainless-steel frames 0.6 mm thick, with a rectangular opening of 150 mm long by 50 mm wide that served as the test area. Each sample was placed vertically at the midplane of the test section. Ignition of the material was induced with a 29-gage Kanthal 45 mm length wire. The igniter is energized using a controlled current power supply (BK Precision 1785) set to deliver 40 W for about 10 s. The igniter was braided along the upstream edge of the sample (bottom of the sample) for the concurrent flames experiments, whereas for the opposed ones it was braided along the downstream edge of the sample (top of the sample). The concurrent spread experiments were repeated five times for each test condition to address the experimental uncertainty, whereas three repetitions were sufficient for downward spreading flames because of their steadiness and higher repeatability.

The ignition and subsequent flame spread were video recorded with a resolution of 1920 by 1080 at 30 frames per second using a Sony RX10-III camera for the front view, and a second camera (Nikon D3200) was used to record videos of the flame side view with a resolution of 1920 by 1080 at 30 frames per second. The camera settings were kept constant among the experiments, although they slightly differ between front view and side view. The experiments videos were processed using a Python-based program, called Flame Tracker, internally developed and now publicly available²⁰. The color tracking method, based on intensity thresholds for each pixel in the RGB channels, was used to isolate the flame region from the background on a frame-by-frame basis, and the minimum and maximum coordinates were identified as flame base and tip locations. The flame length is directly calculated as the difference between these two locations. The Flame Tracker also calculated the spread rates between all the frames considered (both for flame base and flame tip); these values were smoothed with a moving average, with a number of frames between 10 and 30, corresponding to a time average of 0.3 and 1 s. In this work we report the spread rate values of the flame base for the opposed flow configuration, and the ones of the flame tip for the concurrent flow configuration.

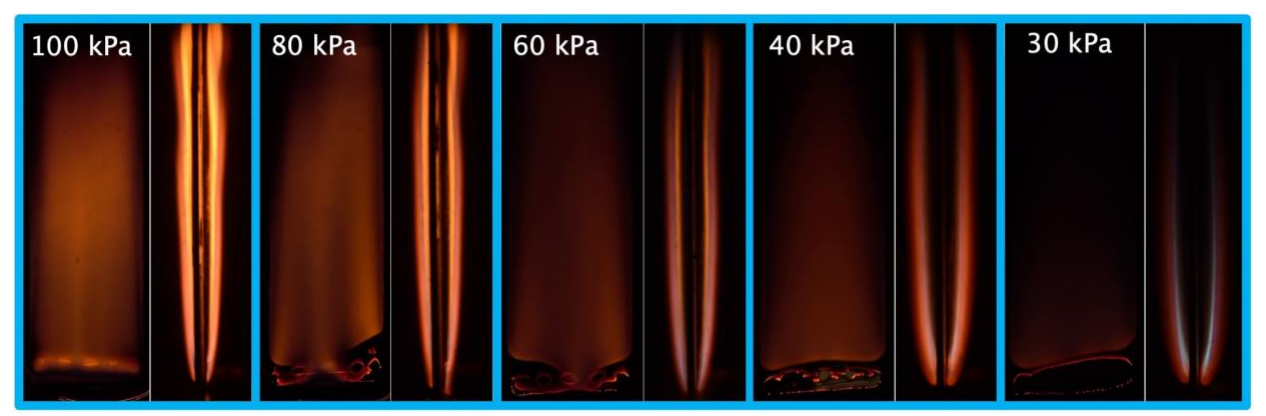


Figure 2. Frontal (left frame) and lateral (right frame) view of concurrent spreading flames over thin cotton samples for the tested pressure levels.

III. Experimental Results

A. Concurrent flames

Figure 2 shows the frontal (on the left) and side (on the right) views of concurrent spreading flames a few seconds after ignition, at the tested pressure levels. Camera settings are maintained constant with variating pressure to qualitatively show the visual differences of the observed flames. From the side flames we can notice that by reducing pressure the flames become dimmer, and the turbulence and flickering at the tip of the flames gradually disappear. From these images we can also notice that the flame region becomes thicker (along the direction perpendicular to the fuel surface) despite the lower luminosity, suggesting that diffusion processes get increasingly important. An interesting feature shown by the photographs of the flames starting at pressures below 60 kPa is the location of the blue portion of the flame. Diffusion flames are controlled by the transport of the fuel and oxidizer toward the reaction zone. Naturally we would expect a larger supply of fresh oxidizer on the outer side of the flame zone (oxidizer side), while we expect a larger fuel concentration in the inner side (fuel side). Consequently, the sooty region of the flame, characterized by the yellow-orange color, develops on the fuel side, while the flame leading edge and the outer layer have a blue color characteristic of CH radicals' emissions in contact with the oxidizer, although usually this layer is not visible because of the much lower luminosity with respect of the sooty region. However, as shown in Figure 2, the blue region of the flame moves towards the fuel side at low pressure. From these images it is not clear if the internal blue layer is not visible at higher pressures or if it is not present at all. A similar effect is visible in the side flames at

reduced pressure in Ref. 10. An inner blue region with an outer red halo was observed also in microgravity flames (drop tower tests) at very low pressures (~5 kPa) by Marcum et al.21; the red region was associated to a two-stage reaction zone following the leak of reactants such as CO and H₂ slowly reacting to CO₂ and H₂O. However, the pressure levels considered in this work are much higher, and by a visual comparison with Ref. 21, the flame inversion might have a different nature, especially since the red region in the flame pictures of Figure 2 seems generated by soot radiation emission. The blue region could indicate that the oxidizer can better penetrate to the fuel side because of the enhanced diffusion at low pressure, or that it could enter from the quenching zone by the flame leading edge; despite the reason, this behavior has not been observed in microgravity.

Upward spreading flames grow over time, and so do their spread rates. Given the total length of the samples

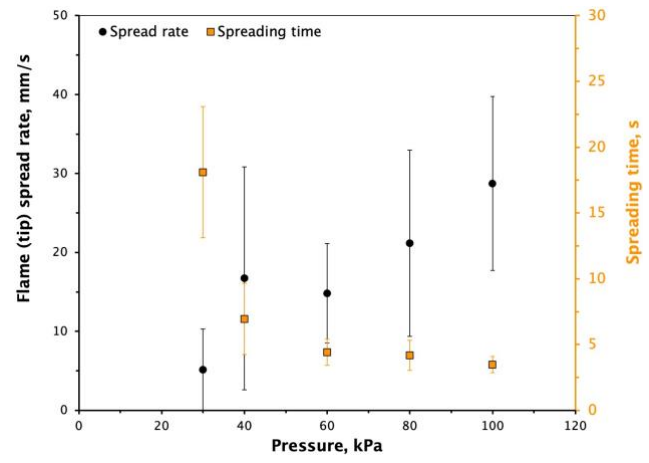


Figure 3. Variation of the spread rate (left axis), and time needed by the flame to cover the entire sample length (right axis) with pressure for upward spreading flames over cotton samples.

considered in this work (about 150 mm), the tip of the flame reached the end of the sample before substantial movements of the flame base. Instantaneous values of the spread rate for the flame tip were obtained from the front videos on a frame by frame basis (starting when the igniter was turned off), and then smoothed by using a moving average of 10 frames (0.3 s) for pressures above 60 kPa, and 30 frames (1 s) for the lower pressure levels. These spread rate values, which increased over time, were then averaged over the time needed by the flame to cover the entire sample, for all the repetitions of the experiments. Figure 3 shows these average spread rate values as function of ambient pressure, as well

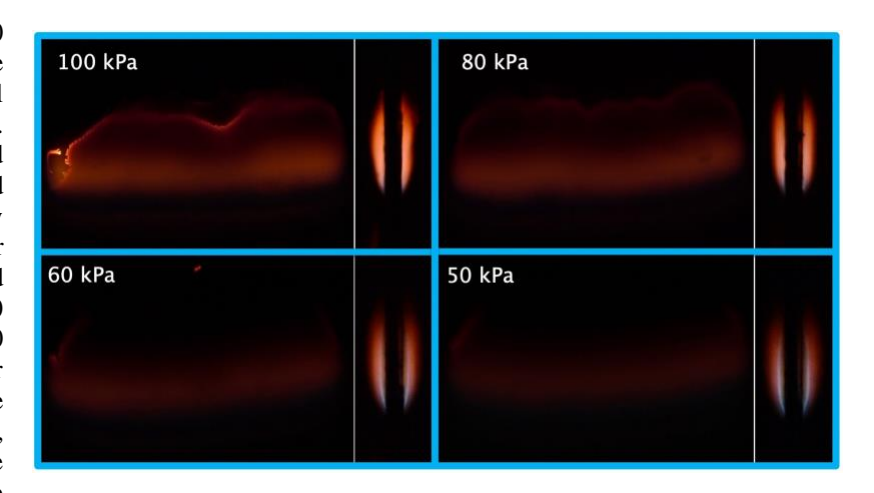


Figure 4. Frontal and lateral views of opposed spreading flames. The spread rate and length of these flames reach steady state soon after ignition.

as the spreading time of the flame tip. The standard deviation reflects the variation of the spread rate values during the experiments, and not among the repetitions; this explains the large error bars. Overall, we can see that the spread rate substantially decreases with pressure, with the only exception being the flames at 40 kPa; these flames tended to shrink after the igniter was turned off, followed by a few seconds of very slow growth before quickly gaining intensity and covering the entire sample. This could be seen as an intermediate behavior between the flames at 60 kPa that grew relatively quickly, and the flames at 30 kPa, which had a much more gradual growth. However, the initial behavior could also be related to a slower ignition process due to the reduced pressure. This transition of flame behavior can also be observed by the spreading times reported in Fig. 3; from 100 kPa to 60 kPa, the flames reached the end of the samples in less than 5 seconds in all cases, with small dependence on pressure. On the other hand, the spreading time starts increasing at 40 kPa, and at 30 kPa it becomes more than four times larger than at 100 kPa.

B. Opposed flames

Figure 4 shows the front and lateral views of opposed spreading flames over the cotton samples about 20 s after ignition at the tested pressure levels. At 40 kPa the flame could not propagate along the sample after ignition, thus in the opposed spread configuration we reached a non-propagation (extinction) limit, while concurrent flames were able to spread at much lower pressures.

As in the concurrent case, by reducing pressure the flames get dimmer, their reaction zone becomes thicker (visible

from the side view), and the blue region develops along the internal layer of the flame between 50-60 kPa. The flame length does not seem to be strongly impacted by pressure reductions.

The opposed spread videos were processed to measure the variation of flame position, length and spread rate in time, which reached steady state soon after ignition, unlike the case of concurrent spreading flames that grew over time. Figure 5 shows the variation of flame spread rate and flame length with pressure, averaged among the experiment repetitions. While the spread rate decreases of about 20 % from 1.20 mm/s at 100 kPa to 0.95 mm/s at 50 kPa, the flame length does not show a clear trend. These results are consistent with the thermal theory of opposed flame spread, which predicts small variations of spread rate with pressure²².

From the comparison of the flame pictures in Figure 2 and Figure 4 (not in the same scale), it is also seen that

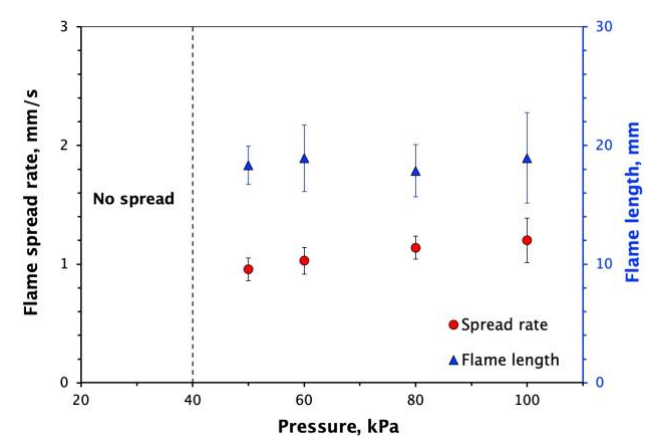


Figure 5. Variation of the measured spread rates (left axis), and flame length (right axis) with pressure for opposed spreading flames.

the flame lengths are much larger for concurrent spreading flames than for opposed spreading flames. This is due to the difference geometrical configuration of the burning surface; in concurrent flame spread a flame spreads on each side of the cotton sheet, the pyrolysis region is determined by the rate of spread of the burning front and the pyrolysis front, and it is followed by a relatively long preheating region downstream of the pyrolysis front²³, where the flames on each side are guided by the momentum boundary layer. In opposed flow flame spread, the solid fuel ends at the burn out edge, and the flames from both sides of the cotton sheet converge into a single flame, burning in a wake type diffusion flame.

C. Standoff distance

The flame standoff distance is an important parameter in flame spread modeling because of its relation to the heat transfer between fuel surface and flame region, and dependence on ambient conditions. A common assumption for flames burning in atmospheric conditions is the flame-sheet approximation (infinitely thin flame), resulting from infinitely fast kinetics and no products dissociation²⁴. In reality, finite-rate chemistry and diffusion cause the flame to have a finite thickness, especially at low pressures. The importance of the standoff distance can vary with the flame

spreading configuration; since the concurrent flames developed over flat fuels cover a much larger fuel area than opposed spreading flames, variations of standoff distance could play a bigger role in the first case.

To quantify the effect of pressure on the standoff distance, the side videos of concurrent flames spreading over the cotton surface were processed to measure the maximum distance from the fuel surface to the outer flame region. Because of the thickness of the flame, we refer to this measured length as maximum flame standoff distance. The measured values for concurrent flames are reported in Figure 6, and error bars are presented showing the variability between repetitions at similar conditions. As mentioned before, the tip of concurrent flames oscillates for pressures between 60-100 kPa, thus only the laminar portion of the flame was considered for the tracking, as shown in the inset of the figure (the shaded upper region was neglected for these measurements). From the graph of Figure 6, we can see that the maximum distance increases of about 50% going from 100 to 30 kPa for concurrent flames.

Figure 6 also presents the results for the flames spreading downward in the opposed flow configuration.

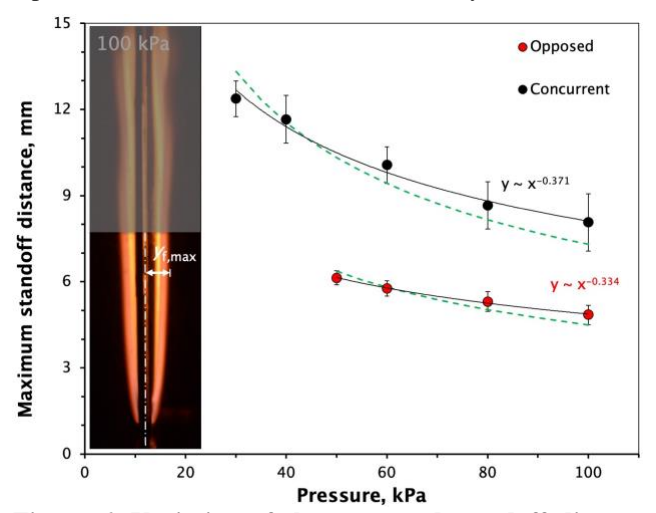


Figure 6. Variation of the measured standoff distance with pressure for concurrent and opposed spreading flames. The green dashed lines represent pressure dependencies of $p^{-0.5}$. The inset shows how the laminar region was considered to measure the maximum distance between fuel surface and flame.

It can be seen that a similar increase in the maximum standoff distance occurs for opposed spreading flames as for concurrent spreading flames in the smaller range 100-50 kPa. Furthermore, from the measurements it was observed that the standoff distance was not function of time, and small oscillations decreased at lower pressures, as indicated by the lower standard deviation in Figure 6 for the values below 50 kPa.

IV. Simplified Analysis and Discussion

In both concurrent and opposed flame spread, the flow velocity approaching the flame region is an important parameter of the problem since it controls the residence time of the oxidizer. The flames tested in this work were exposed to a forced flow velocity of 20 cm/s, and the buoyant flow generated by these flames is of the same order of magnitude (10-50 cm/s). Thus, the flow velocity affecting the boundary layer along the sample and the flame itself are exposed to a mixed (forced and free) flow. This type of situation has been previously studied theoretically²⁵⁻²⁷. Specifically, a relation for the flame standoff distance y_f was derived in terms of non-dimensional parameters²⁷:

$$y_f = (\text{Re}^4 + \text{Gr}^2)^{-1/8} x \int_0^{\eta_f} \left[1 + \theta \left(\frac{T_w}{T_\infty} - 1 \right) \right] d\eta$$
 (1)

With Re = $V_g x/v$ being the Reynolds number, Gr = $g\beta\Delta T x^3/v^2$ the Grashof number, θ a non dimensional temperature parameter, and x the local coordinate along the fuel; the other parameters are kinematic viscosity (v), flow velocity (V_g), gravity (g), thermal expansion coefficient (β), the integration variable for the coordinate y (η), the wall and ambient temperatures (T_w and T_∞), and temperature difference between flame and surroundings (ΔT). The standoff distance increases with the coordinate along the sample x, but this is not the case for opposed spreading flames, where the flames on each side of the sample reattach after the pyrolysis region, as discussed in Sec. III.B (see Figure 4). However, since we are interested in the flame leading edge region, which is the one determining the spread along the sample, we can ignore the wake region of opposed spreading flames for this analysis.

For simplicity, we can assume a constant value of the coordinate x in Eq. (1), equal to a length scale of the problem L. Reynolds and Grashof numbers in Eq. (1) may be described by different characteristic lengths; the development length of the boundary layer in front of the flame determines Re, while the Gr number measures the buoyant flow generated by the flame, with length scales of the order of pyrolysis or flame lengths. However, in first approximation we can assume a single characteristic length. Moreover, the integral term in Eq. (1) is of order 1 and does not dependent on pressure, thus we can rewrite Eq. (1) as:

$$y_f \sim (\text{Re}^4 + \text{Gr}^2)^{-1/8} L$$
 (2)

This equation is valid for a mixed flow, and in the cases where $Re \gg Gr$, or $Gr \gg Re$, we would obtain respectively the standoff variation in a flow dominated by the forced or buoyant components.

The buoyant flow induced by a flame is given by the density difference between the flame region and the surroundings. Therefore, we can rewrite the Grashof number in terms of the density difference between the flame region and the surrounding environment. The pressure dependencies of Gr and Re become:

$$Gr = g\rho\Delta\rho L^3/\mu^2 \rightarrow \rho\Delta\rho = \rho_\infty(\rho_\infty - \rho_f) \sim p_\infty^2$$
(3)

$$Re = \rho V_a L / \mu \sim p_{co} \tag{4}$$

The density of the flame region ρ_f is much lower than the ambient density because of the high temperature, therefore we expect a low dependence of ρ_f on the ambient pressure, therefore $\rho_{\infty} - \rho_f \propto p_{\infty}$. By substituting the pressure dependencies from Eq. (3) and (4) in Eq. (2), we can estimate the variation of the standoff distance with pressure to be $y_f \sim p^{-0.5}$. By applying a power law fitting to the measured values of the maximum standoff distance in Figure 6, we obtain a pressure exponent of -0.33 in the case of opposed spreading flames, and -0.37 in the case of concurrent spreading flames. The green dashed lines in Figure 6 correspond to a $p^{-0.5}$ dependence, and they fit within the error bars of the experimental results. Given the limitations in measuring the standoff distance, e.g. the change of flame luminosity with pressure, and the thickening flame region in contrast with an infinitely thin flame sheet approximation (infinitely fast kinetics), the predicted and measured exponents are reasonably close. Furthermore, the length scale of the problem in Eq. (2) could vary with pressure as well and could be responsible of the difference in the pressure exponent.

The importance of the length scales of the problem depends on the spreading configuration. The flame length of opposed spreading flames does not significantly affect the fuel ahead of the flame, whereas in concurrent spreading flames a longer flame preheats more fuel to the vaporization temperature. The pyrolysis length, on the other hand, is proportional to the spread rate for both opposed and concurrent spreading flames; this length is also an appropriate scale to estimate the buoyant flow induced by the flames. By using the definitions of Reynolds and Grashof numbers in Eq. (3) and (4), and the pyrolysis length L_p as the characteristic length of the problem, Eq. (2) becomes:

$$y_f \sim \left(\frac{L_p \mu_\infty}{\rho_\infty}\right)^{1/2} \left(V_g^4 + g^2 L_p^2 \frac{\Delta \rho^2}{\rho_\infty^2}\right)^{-1/8}$$
 (5)

We can estimate the variation of the standoff distance with the experimental conditions of $V_g = 20$ cm/s, $g = 9.81 \text{m/s}^2$, density and viscosity calculated at the ambient temperature ($T_{\infty} = 300$ K), respectively 1.16 kg/m³ and 1.85·10⁻⁵ kg/(m·s), and by assuming a constant density in the flame region of 0.17 kg/m³ obtained at a flame temperature of 2100 K. The value of the pyrolysis length L_p changes between the spreading configurations. Furthermore, previous experiments for concurrent spread have shown that L_p is function of pressure⁷, but since in this

work we consider the standoff distance for the developed flame, it is reasonable to assume that the flame already spread through the entire sample, and therefore $L_p=150\,\mathrm{mm}$. The pyrolysis length is function of pressure also for opposed spreading flames, but its variation is negligible for the thin samples presented in this work. Thus, for simplicity we can select a constant value of $10~\mathrm{mm}$ (same order of magnitude of the experimental values).

Figure 7 shows the comparison between the experimental values from Figure 6, and the values estimated from Eq. (5) with a multiplication factor of 5. It is interesting to notice that the standoff distance for opposed flames follows the same trend of the values for concurrent flame spread, despite the fundamental differences between these two configurations.

V. Conclusion

Experiments of opposed and concurrent flame spread configurations were carried on over thin cotton

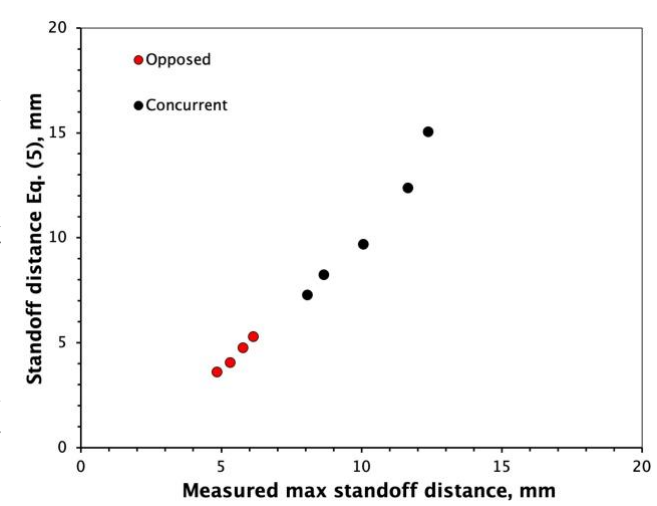


Figure 7. Correlation between Eq. (5), multiplied by a factor of 5, and the measured values of the maximum standoff distance, for both opposed and concurrent spreading flames.

samples at ambient pressure between 30-100 kPa. Overall, a pressure reduction slows down the flame spread, makes the flames dimmer, and causes a thickening of the reaction zone and an increase of flame standoff distance. It was found that opposed flames were not able to spread after ignition at 40 kPa, even though the spread rate at 50 kPa is still close to the one at 100 kPa; this suggests that low pressure extinction is not a gradual behavior, but rather a sudden mechanism that could be due to the effect of pressure on the flame structure and the fuel surface preheating.

Interestingly, at 60 kPa a thin blue region appears near the middle of the diffusion flame, and as the pressure is reduced this blue region moves towards the fuel surface. This is in contrast with common diffusion flames at atmospheric pressure where the blue region is on the oxidizer side of the flame.

The standoff distance, measured as the maximum distance of the flame region from the fuel surface, increases in both opposed and concurrent spread at lower pressures. A simplified analysis is used to study the pressure dependence of the standoff distance for a mixed (forced and free) flow, and the result of $p^{-0.5}$ is close to the experimental values for opposed spread ($p^{-0.33}$), and concurrent spread ($p^{-0.37}$). The difference could be attributed to the characteristic length of the problem, that could vary with pressure as well.

By assuming a constant length equal to the pyrolysis length based on the spread configuration, the flame standoff distance was estimated for the tested conditions. The measured values show good agreement with the estimated values; moreover, opposed and concurrent spreading flames showed a common trend, despite the different order of magnitude of the pyrolysis length.

The results of the standoff distance, and the comparison between opposed and concurrent spreading flames, could be used in future models to estimate the variation of heat flux between fuel and surface at low pressure. Numerical results could clarify the buoyant flow field generated by these flames.

Acknowledgments

This research was supported by NASA Grant NNX12AN67A. The authors would like to thank Prof. Yuji Nakamura for the interesting discussions on the flame structure at low pressure.

References

¹NASA, "Recommendations for Exploration Spacecraft Internal Atmospheres: The Final Report of the NASA Exploration Atmospheres Working Group," NASA/TP-2010-216134, 2010.

²Olson, S. L., Kashiwagi, T., Fujita, O., Kikuchi, M., Ito, K., "Experimental observations of spot radiative ignition and subsequent three-dimensional flame spread over thin cellulose fuels," *Combust. Flame*, Vol. 125, No. 1-2, 2001, pp. 852–864.

³Olson, S. L., "Mechanisms of Microgravity Flame Spread Over a Thin Solid Fuel: Oxygen and Opposed Flow Effects," *Combust. Sci. Technol.*, Vol. 76, No. 4-6, 1991, pp. 233–249.

- ⁴Olson, S. L., Ferkul, P. V., "Microgravity flammability boundary for PMMA rods in axial stagnation flow: Experimental results and energy balance analyses," *Combust. Flame*, Vol. 180, June 2017, pp. 217–229.
- ⁵Olson, S. L., Ferkul, P. V., T'ien, J. S., "Near-limit flame spread over a thin solid fuel in microgravity," *Symp. (Int.) Combust.* 22, No. 1, 1989, pp. 1213–1222.
- ⁶ Fereres, S., Lautenberger, C., Fernandez-Pello, C., Urban, D. L., Ruff, G. A., "Understanding ambient pressure effects on piloted ignition through numerical modeling," *Combust. Flame*, Vol. 159, No. 12, 2012, pp. 3544-3553.
- ⁷Thomsen, M., Fernandez-Pello, C., Urban, D. L., Ruff, G. A., Olson, S. L., "On simulating concurrent flame spread in reduced gravity by reducing ambient pressure," *Proc. Combust. Inst.*, Vol. 37, No. 3, 2019, pp. 3793-3800.
- ⁸Thomsen, M., Fernandez-Pello, C., Ruff, G. A., Urban, D. L., "Buoyancy effects on concurrent flame spread over thick PMMA," *Combust. Flame*, Vol. 199, Jan. 2019, pp. 279-291.
- ⁹Nakamura, Y., Yoshimura, N., Ito, H., Azumaya, K., Fujita, O., "Flame spread over electric wire in sub-atmospheric pressure," *Proc. Combust. Inst.*, Vol. 32, No. 2, 2009, pp. 2559-2566.
- ¹⁰Kleinhenz, J., Feier, I. I., Hsu, S.-Y., T'ien, J. S., Ferkul, P. V., Sacksteder, K. R., "Pressure modeling of upward flame spread and burning rates over solids in partial gravity," *Combust. Flame*, Vol. 154, No. 4, 2008, pp. 637-643.
- ¹¹Ferkul, P. V., T'ien, J. S., "A model of low-speed concurrent flow flame spread over a thin fuel," *Combust. Sci. Technol.*, Vol. 99, No. 4-6, 1994, pp. 345–370.
- ¹²Hsua, S.-Y., T'ien, J. S., "Pressure extinction limits of non-premixed flames," *Combust. Th. Model.*, Vol. 13, No. 5, 2009, pp. 885-900
- ¹³Bhattacharjee, S., Carmignani, L., "Radiation-kinetics interactions: A comparison of opposed-flow flame spread in a low-velocity microgravity and low-pressure downward environments," *Proc. Combust. Inst.*, (In press), 2020.
- ¹⁴Altenkirch, R. A., Eichhorn, R., Shang, P. C., "Buoyancy Effects on Flames Spreading Down Thermally Thin Fuels," *Combust.* Flame, Vol. 37, 1980, pp. 71-83.
- ¹⁵Mao, C.-P., Kodama, H., Fernandez-Pello, A. C., "Convective Structure of a Diffusion Flame over a Flat Combustible Surface," *Combust. Flame*, Vol. 57, 1984, pp. 209-236.
- ¹⁶Zhang, Y., Ronney, P. D., Roegner, E. V., Greenberg, J. B., "Lewis Number Effects on Flame Spreading Over Thin Solid Fuels," *Combust. Flame*, Vol. 90, 1992, pp. 71-83.
- ¹⁷Zarzecki, M., Quintiere, J. G., Lyon, R. E., Rossmann, T., Diez, F. J., "The effect of pressure and oxygen concentration on the combustion of PMMA," *Comb.* Flame, Vol. 160, 2013, pp. 1519-1530.
- ¹⁸Zhao, K., Zhou, X., Liu, X., Tang, W., Gollner, M., Peng, F., Yang, L., "Experimental and theoretical study on downward flame spread over uninhibited PMMA slabs under different pressure environments," *App. Therm. Engin.*, Vol. 136, 2018, pp. 1-8.
- ¹⁹Thomsen, M., Fernandez-Pello, C., Huang, X., Olson, S., Ferkul, P., "Buoyancy Effect on Downward Flame Spread Over PMMA Cylinders," *Fire Technol.*, Vol. 56, Jan. 2020, pp. 247-269.
- ²⁰Carmignani, L., "Flame Tracker: an image analysis program to measure flame characteristics," *SoftwareX*, April 2021 (submitted), https://github.com/combustionTools/flameTracker.
- ²¹Marcum, J. W., Rachow, P., Ferkul, P. V., Olson, S. L., "Low pressure flame blowoff of the stagnation region of cast PMMA cylinders in axial mixed convective flow," *Combust. Flame*, Vol. 216, June 2020, pp. 385-397.
 - ²² Wichman, I.S., "Theory of opposed-flow flame spread," *Prog. En. Combust. Sci.*, Vol. 18, pp.553-593.
 - ²³Markstein, G. H., de Ris, J., "Upward fire spread over textiles," Symp. (Int.) Combust., Vol. 14, No. 1, 1973, pp. 1085-1097.
 - ²⁴Williams, F. A., "Theory of combustion in laminar flows," *Annual Review Fluid Mech.*, Vol. 3, Jan. 1971, pp. 171-188.
- ²⁵Fernandez-Pello, A. C., "A Theoretical Model for the Upward Laminar Spread of Flames Over Vertical Fuel Surfaces," *Combust. Flame*, Vol. 31, 1978, pp. 135-148.
 - ²⁶Fernandez-Pello, A. C., "Flame Spread in a Forward Forced Flow," Combust. Flame, Vol. 36, 1979, pp. 63-78.
- ²⁷Mao, C. P., Fernandez-Pello, A. C., Pagni, P. J., "Mixed Convective Burning of a Fuel Surface with Arbitrary Inclination," *J. Heat Transf.*, Vol. 106, No. 2, 1984, pp. 304-309.